Empirical Validation and Certification of Prime Curvature Geometry

Bill C. Riemers

January 24, 2026

Abstract

This paper presents an empirical certification of the **Prime Curvature Geometry Conjecture for Goldbach (PCGC–Goldbach)**, as formulated in [6]. All tested instances with $4 \leq 2n \leq 23\# \approx 2.5852 \times 10^8$ are certified to satisfy the geometric curvature bounds predicted by PCGC–Goldbach. The certification spans a discrete family of fixed-scale Goldbach windows and covers more than 16 billion non-trivial test scenarios, with no violations observed across the entire tested range.

Beyond aggregate verification, the paper provides detailed extremal and pointwise analysis of the certified bounds together with a fully reproducible computational pipeline. All certified claims are grounded in explicit enumeration rather than probabilistic heuristics, and the associated data products and verification artifacts are archived to permit independent audit and falsification.

Contents

1 Introduction

1.1 Background

The Prime Curvature Geometry Conjecture for Goldbach (PCGC–Goldbach) was introduced in [6] as a geometric framework for bounding deviations in Goldbach pair counts. The present paper reports an empirical certification of that framework over a large, explicitly enumerated domain.

Crucially, the original intent of the computational programme was *not* to verify pointwise validity of PCGC–Goldbach. On the contrary, the working assumption motivating the software design was that prime distributions exhibit pseudo-random behaviour at sufficiently fine scales, and that any non-aggregated formulation of the conjecture would almost certainly admit local violations.

Under this assumption, one expects bounds derived from a geometric approximation to hold only after aggregation over intervals large enough to be statistically representative, and to fail when tested pointwise in n. Accordingly, the computational framework was engineered to probe a wide range of window sizes and aggregation regimes, with the expectation that sufficiently fine partitions would expose outliers.

Only after observing *zero* violations across all tested cross-intervals $\Delta_\alpha(n)$, spanning 81 distinct curvature parameters α, did it become clear that this expectation of statistical failures was incorrect. Rather than exhibiting sporadic pointwise escapes, the measured pair counts remain uniformly confined within the predicted curvature envelopes.

To verify that the absence of violations was not an artifact of the computational pipeline, controlled perturbation tests were performed designed to force failures. Specifically, key structural components of the PCGC–Goldbach framework were deliberately replaced with known-inadequate surrogates. In particular, the effective local modulus $\mathcal{Q}_p(n)$ was replaced by the corresponding primorial cutoff $p\#$, thereby discarding the adaptive localisation that encodes small-prime congruence structure.

Under these substitutions, violations of the predicted bounds appeared immediately and systematically, both in aggregated extrema and at the pointwise level. The resulting failure patterns were consistent with theoretical expectations and confirm that the software reliably detects genuine departures from admissible curvature.

These perturbation tests demonstrate that the observed absence of violations under the full PCGC–Goldbach formulation is not a consequence of numerical smoothing, windowing artefacts, or implicit aggregation, but reflects a structural property of the conjectured geometry itself. Thus, the empirical results do not arise from tuning the experiment to

confirm a conjecture, but instead from an outcome that directly contradicts the original working hypothesis built into the experimental design.

1.2 Computational Framework Overview

The software used in this study is an extension of the framework introduced in [4]. As before, binning is performed using primorial-based windows, preserving compatibility with Hardy–Littlewood–style local corrections.

Two operational modes are supported:

1. *Aggregated mode*, in which Hardy–Littlewood windowed predictions and measured pair counts are generated in separate runs. In this configuration, pointwise verification is not possible, but global extrema can be rigorously compared.
2. *Combined mode*, in which predicted bounds and measured values are evaluated jointly, enabling pointwise certification.

In aggregated mode, prediction runs complete in approximately half a day on an Apple M2 processor, while full pair-count runs require approximately six days. Combined mode additionally requires evaluating high-precision logarithmic products for each admissible odd-pair candidate and consequently incurs a computational cost approximately an order of magnitude greater than standard Goldbach pair counting.

Across all tested primorial bins, no violations of the predicted bounds were observed. Moreover, the extremal values of the normalised log-ratio

$$\log(G/\mathring{G}) \tag{1}$$

exhibit local fluctuations but show an overall tightening trend toward zero across the tested range.

1.3 Contributions

The principal contributions of this paper are as follows:

- Provide an empirical certification of the Prime Curvature Geometry Conjecture for Goldbach over the range $4 \leq 2n \leq 23\#$, covering a discrete family of 81 fixed-scale window parameters and more than 16 billion non-trivial test scenarios.

- Demonstrate that the predicted geometric curvature bounds hold not only in aggregated regimes but also pointwise, with no observed violations across the entire certified domain.
- Introduce a reproducible certification methodology that treats geometric bounds as falsifiable numerical claims, supported by explicit enumeration, archived data products, and independently auditable verification logs.
- Validate the sensitivity of the computational pipeline through controlled perturbation tests, confirming that violations are reliably detected when essential geometric structure is removed.
- Clearly delineate the scope of the certification, distinguishing the fixed-scale regime studied here from geometrically distinct short-interval problems that require separate analytical and experimental treatment.

2 Fundamental Definitions and Identities

The definitions and identities collected in this section are adapted from [5, 6]. They are presented here in a condensed form sufficient for the present work; for full derivations, motivation, and extended discussion, the reader is referred to the cited papers.

2.1 Admissible Parity

The parity restriction was introduced in [5]. Here it is used purely as an admissibility convention for windowed sums and products.

Definition 1 (Parity–Admissible Window Index Set)**.**
Let $n \in \mathbb{N}$ and let $M \in [0, n]$. Define the symmetric window

$$I_M := \{\, m \in \mathbb{Z} : 0 < |m| \le M \text{ and } 3 \le n - |m| \,\}. \tag{2}$$

The *parity–admissible index set* is

$$I^{\mathrm{par}}(n; M) := \{\, m \in I_M : n + m \equiv 1 \pmod 2 \,\}. \tag{3}$$

Equivalently, $I^{\mathrm{par}}(n; M)$ consists of those shifts m with $0 < |m| \le M$ for which both $n - m$ and $n + m$ are odd integers at least 3. Unless stated otherwise, all summations over window variables m in this paper are implicitly restricted to $m \in I^{\mathrm{par}}(n; M)$.

Definition 2 (Euler–Cap Operator)**.**
The PCGC–Goldbach conjecture is formulated only for *Euler–cap admissible* window radii. To allow formulas to be written uniformly in terms of an unconstrained window parameter, the following coercion operator is introduced.

Fix $n \in \mathbb{N}$. For any $M \geq 0$ measured in the same units as the window radius, define

$$\langle M \rangle_{\mathrm{ec}} \;:=\; \lfloor \min(M,\, \mathrm{Ecap}(n)\, n) \rfloor \;=\; \left\lfloor \min\left(M,\, \frac{(2n+1) - \sqrt{8n+1}}{2} \right) \right\rfloor . \tag{4}$$

Thus $\langle M \rangle_{\mathrm{ec}}$ denotes the largest Euler–cap admissible window radius not exceeding M.

Convention. The Euler–cap operator $\langle \cdot \rangle_{\mathrm{ec}}$ enforces admissibility of window parameters. This paper assumes the Euler cap is applied globally and will therefore not be explicitly specified.

2.2 Effective Local Moduli

Definition 3 (Effective Local Modulus)**.**
Let $n \in \mathbb{N}$ and let p be an odd prime. Define the minimum contributing prime by

$$p_{\min}(n) := \begin{cases} 3, & 3 \mid n, \\ 5, & 3 \nmid n. \end{cases} \tag{5}$$

For each $n \geq 2$, let

$$\mathbb{P}_{\mathrm{eff}}(n) := \{\, p \in \mathbb{P} : p \geq \mathrm{p}_{\min}(n) \,\}. \tag{6}$$

We regard $\mathcal{Q}_p(n)$ as defined only for $p \in \mathbb{P}_{\mathrm{eff}}(n)$.

For any odd prime $q_{\min}$, define the partial Euler product

$$\mathcal{Q}_p^{(q_{\min})} := \prod_{\substack{q \in \mathbb{P} \\ q_{\min} \leq q \leq p}} (q-1). \tag{7}$$

The *effective local modulus* at p for the even integer $2n$ is then

$$\mathcal{Q}_p(n) := \mathcal{Q}_p^{\left(p_{\min}(n)\right)}. \tag{8}$$

Thus $\mathcal{Q}_p(n)$ encodes the cumulative residue structure imposed by the odd primes below p, with the only n-dependence arising from the choice of base prime $p_{\min}(n)$ according to whether $3 \mid n$. This convention is tailored to the singular–series geometry underlying Goldbach–type problems.

Definition 4 (Effective Moduli Interval Max)**.**

$$\mathcal{Q}(2n; L) := \mathcal{Q}_{P_0(2n;L)}(n), \tag{9}$$

$$P_0(2n; L) := \max\{\, p \in \mathbb{P}_{\text{eff}}(n) : \; p \mid n, \mathcal{Q}_p(n) \le L \,\}, \tag{10}$$

$$\text{with } P_0(2n; L) := \mathrm{p}_{\min}(n) \text{ if the set is empty.} \tag{11}$$

2.3 Prime Curvature Constants

The prime curvature constants encode the cumulative medium– and large–prime contribution to the geometric remainder envelope.

Definition 5 (Prime Curvature Constants)**.**
Fix the base prime $q_{\min} = 5$, and recall the auxiliary effective moduli $\mathcal{Q}_p^{(5)}$ from Definition 3. Define the *prime curvature constant* by the convergent Euler product

$$\Omega_{\text{prime}} := \prod_{p \in \mathbb{P}_{\text{eff}}(5)} (p-2)^{1/\mathcal{Q}_p^{(5)}} \tag{12}$$

For each even integer $2n$ and Euler–cap admissible window scale L, define the *renormalized prime curvature factor* by

$$\widehat{\Omega}_{\text{prime}}(2n; L) := \Omega_{\text{prime}}^{\kappa(n)} \prod_{\substack{p \in \mathbb{P}_{\text{eff}}(n) \\ \mathcal{Q}_p(n) \le L}} (p-2)^{-1/\mathcal{Q}_p(n)} \tag{13}$$

where the exponent $\kappa(n) \in \{\frac{1}{2}, 1\}$ compensates for the choice of base prime $\mathrm{p}_{\min}(n) \in \{3, 5\}$ in Definition 3.

Specifically, when $3 \nmid n$ one has $\mathrm{p}_{\min}(n) = 5$ and $\kappa(n) = 1$. When $3 \mid n$, the extra contribution from the prime 3 is absorbed into the exponent $\kappa(n) = \frac{1}{2}$.

Definition 6 (Bounding Envelope Constants)**.**
Then the envelope for $L \ge \mathrm{p}_{\min}(n)$ constant is given explicitly by

$$c(2n; L) = c\big(2n; \mathcal{Q}_p(n)\big) \;=\; 2 \prod_{\substack{q \in \mathbb{P}_{\text{eff}}(n) \\ \mathcal{Q}_q(n) > \mathcal{Q}_p(n)}} (q-2)^{\,\mathcal{Q}_p(n)/\mathcal{Q}_q(n)}. \tag{14}$$

In particular, $c(2n; L)$ is constant on each envelope interval $[\mathcal{Q}_p(n),\, \mathcal{Q}_{p^+}(n))$.

2.4 Goldbach Singular Series Factors

Definition 7 (Goldbach Singular Series Factors)**.**
For an even integer $2n$, the *local semiprime correction factor* [2] is defined as

$$\mathfrak{S}(2n) := \prod_{\substack{p \mid n \\ p>2}} \frac{p-1}{p-2}. \tag{15}$$

Define the *prime–pair constant* [2] by

$$C_2 := \prod_{p>2} \left(1 - \frac{1}{(p-1)^2}\right). \tag{16}$$

The corresponding *Goldbach singular series factor* [2] is

$$\mathfrak{S}_{\mathrm{GB}}(2n) := 2\, C_2\, \mathfrak{S}(2n). \tag{17}$$

Definition 8 (Hardy-Littlewood Circle Method Correction Factor)**.**
For $n \geq 2$ and $n > M \geq 1$, and a weight function $\frac{1}{\log n}$, define,

$$\mathcal{H}(2n; M) := \frac{1}{|I^{\mathrm{par}}(n, M)|} \sum_{m \in I^{\mathrm{par}}(n,M)} \frac{\log^2 n}{\log(n-m)\log(n+m)}. \tag{18}$$

Definition 9 (Measured Goldbach Count)**.**
The measured number of Goldbach pairs in the window is

$$G(2n; M) := \sum_{m \in I^{\mathrm{par}}(n,M)} 1_{\mathrm{prime}}(n-m)\, 1_{\mathrm{prime}}(n+m). \tag{19}$$

Definition 10 (Hardy–Littlewood Window Predictor (Hl–Windowed))**.**
Assume the standard prime weight (e.g. $\omega(x) = 1/\log x$). Define

$$\mathring{G}^{\mathrm{HL}}(2n; M) := 2\, C_2\, \mathfrak{S}(2n) \frac{2M}{\log^2 n}\, \mathcal{H}(2n; M). \tag{20}$$

where $\mathfrak{S}(2n)$ is the classical Hardy–Littlewood semiprime correction.

2.5 Complementary and Full Euler–Type Products

In addition to the local semiprime correction factor $\mathfrak{S}(2n)$ defined above, it is occasionally convenient to refer to the complementary and full Euler–type products obtained by modifying the divisibility condition on the prime index.

Definition 11 (Complementary and Full Local Semiprime Products)**.**
Define the *complementary* local semiprime product by

$$\mathfrak{S}^{\complement}(2n) := \prod_{\substack{p\in\mathbb{P}\setminus\{2\}\\ p\nmid n}} \frac{p-1}{p-2}, \tag{21}$$

and the corresponding *full* product by

$$\mathfrak{S}^{\bullet}(2n) := \prod_{p\in\mathbb{P}\setminus\{2\}} \frac{p-1}{p-2}. \tag{22}$$

Convention (Notation). A superscript $\complement$ indicates replacement of the divisibility condition $p \mid n$ by $p \nmid n$, while a superscript $\bullet$ indicates removal of the divisibility condition entirely. No additional structure is implied.

2.6 Additional Series Operators

The classical Hardy–Littlewood singular series $\mathfrak{S}(2n)$ is naturally an asymptotic object. For finite–window analysis it is convenient to introduce auxiliary operators that partition the series into base and tail components relative to a square cutoff.

Definition 12 (Cutoff Operators)**.**
The square cutoff operator is defined as

$$\mathsf{Sq}(x) := x^2. \tag{23}$$

The function $\mathcal{Q}(\cdot)$ may also be used as a cutoff operator.

The tags $_{\text{head}}$ and $_{\text{tail}}$ denote the base (small–prime) and tail (large–prime) components relative to a given cutoff.

Definition 13 (Cutoff Components of $\mathfrak{S}$)**.**
Let $M > 0$ and $n \geq 2$. Then, cutoff terms are defined as

$$\mathfrak{S}^{\mathsf{Sq}}_{\text{head}}(2n;M) := \prod_{\substack{p\in\mathbb{P}\setminus\{2\}\\ p\mid n\\ p^2\leq M}} \frac{p-1}{p-2}, \qquad \mathfrak{S}^{\mathsf{Sq}}_{\text{tail}}(2n;M) := \prod_{\substack{p\in\mathbb{P}\setminus\{2\}\\ p\mid n\\ p^2> M}} \frac{p-1}{p-2}. \tag{24}$$

$$\mathfrak{S}^{\mathcal{Q}}_{\text{head}}(2n;L) := \prod_{\substack{p\in\mathbb{P}_{\text{eff}}(n)\\ p\mid n\\ \mathcal{Q}_p(n)\leq L}} \frac{p-1}{p-2}, \qquad \mathfrak{S}^{\mathcal{Q}}_{\text{tail}}(2n;L) := \prod_{\substack{p\in\mathbb{P}_{\text{eff}}(n)\\ p\mid n\\ \mathcal{Q}_p(n)> L}} \frac{p-1}{p-2}. \tag{25}$$

$$\mathfrak{S}^{\mathsf{Sq}}(2n) := \mathfrak{S}(2n), \qquad \mathfrak{S}^{\mathcal{Q}}(2n) := \prod_{\substack{p \in \mathbb{P}_{\mathrm{eff}}(n) \\ p \mid n}} \frac{p-1}{p-2}. \tag{26}$$

Empty products are interpreted as 1.

2.7 Specialized Remainder Decomposition

This leads up to the PCGC–Goldbach Remainder.

Definition 14 (PCGC–Goldbach Remainder)**.**
Define for $M > 0$,

$$R^{\mathrm{HL}}(2n; L) := 2\,\frac{\mathcal{Q}(2n; L)}{\mathfrak{S}^{\mathcal{Q},\complement}_{\mathrm{head}}(2n; L)}\,\big(\widehat{\Omega}_{\mathrm{prime}}(2n; L)\big)^{L}, \qquad L := \sqrt{2M} \tag{27}$$

$$= 2\,\frac{\mathcal{Q}(2n; L)}{\mathfrak{S}^{\mathcal{Q},\complement}_{\mathrm{head}}(2n; L)}\,\Xi(2n; L), \qquad \Xi(2n; L) := \big(\widehat{\Omega}_{\mathrm{prime}}(2n; L)\big)^{L}. \tag{28}$$

The associated bounding envelope is defined as:

Definition 15 (PCGC–Goldbach Bound Envelope)**.**
Define for $2M \geq (\mathrm{p}_{\min}(n) - 1)^2$,

$$\widehat{R}^{\mathrm{HL}}(2n; L) := \frac{c(2n; L)\,L}{\mathfrak{S}^{\mathcal{Q},\complement}_{\mathrm{head}}(2n; L)}, \qquad L := \sqrt{2M}. \tag{29}$$

Role of the Remainder Bound

Lemma (Overall Bounding Envelope) of [5] shows that

$$R^{\mathrm{HL}}(2n; L) \leq \widehat{R}^{\mathrm{HL}}(2n; L) \tag{30}$$

for all admissible L. The purpose of $\widehat{R}^{\mathrm{HL}}$ is therefore *pointwise control* (a certified upper bound), not approximation. In particular, $\widehat{R}^{\mathrm{HL}}$ does not satisfy $\widehat{R}^{\mathrm{HL}}(2n; L)/R^{\mathrm{HL}}(2n; L) \to 1$, and will overestimate some values of $R^{\mathrm{HL}}(2n; L)$ by a scale-dependent factor.

2.8 Empirical Hl-Normalized Measurements

Definition 16 (Empirical Hl-Normalized Measurements (from Semiprime Survivors))**.** Defining the measured (pairs-scale) normalization factor

$$C(2n; n\alpha) \;:=\; \frac{\log^2 n}{n\alpha}\, \mathring{G}^{\mathrm{HL}}(2n; n\alpha), \tag{31}$$

where $n\alpha$ denotes the Goldbach window half-width used in the measurement.

For **primorial-based binning**, small values are treated separately: for $n < 15$, bins are singletons $[k, k+1)$, $k = 1, \ldots, 14$; for $15 \le n < 30$, a single block $[15, 30)$ is used.

For $n \ge 30$, let $p < q$ be consecutive primes with corresponding primorials $p\#$ and $q\#$. Each primorial plateau $[p\#, q\#)$ is partitioned into bins of width

$$w_p := \max\Big(15, \frac{p\#}{2p}\Big), \qquad L_p := q\# - p\#, \qquad K_p := \Big\lceil \frac{L_p}{w_p} \Big\rceil. \tag{32}$$

Then nodes are defined as

$$a_j := p\# + \min(j\, w_p,\, L_p), \qquad j = 0, 1, \ldots, K_p, \tag{33}$$

so that $a_0 = p\#$ and $a_{K_p} = q\#$. The indexed primorial bins are

$$B_{j,p\#} := [\, a_j,\ a_{j+1}\,), \qquad j = 0, 1, \ldots, K_p - 1, \tag{34}$$

forming consecutive intervals of width w_p, with the final bin truncated so that its right endpoint is exactly $q\#$.

Within each primorial bin $B_{j,p\#}$, with n ranging over integers in the bin, define

$$N_0 := \arg\min_{n \in B_{j,p\#}} C(2n; n\alpha), \qquad N_1 := \arg\max_{n \in B_{j,p\#}} C(2n; n\alpha), \tag{35}$$

and

$$C_{\min}(j, p\#) := C(2N_0; n\alpha), \tag{36}$$

$$C_{\max}(j, p\#) := C(2N_1; n\alpha), \tag{37}$$

$$C_{\mathrm{avg}}(j, p\#) := \frac{1}{|B_{j,p\#}|} \sum_{n \in B_{j,p\#}} C(2n; n\alpha). \tag{38}$$

3 Main Conjecture

3.1 PCGC–Goldbach

This work is to verify the PCGC–Goldbach, introduced in [6] over a finite range of data.

Conjecture 1 (Prime Curvature Conjecture for Goldbach (Pcgc–Goldbach))**.**
For every even integer $2n \geq 4$ and every admissible window size Euler Capped M, the Goldbach pair counts satisfy

$$\left|G(2n; M) - \mathring{G}^{\mathrm{HL}}(2n; M)\right| \leq R^{\mathrm{HL}}(2n; L), \qquad L := \sqrt{2M}, \tag{39}$$

where the remainder term $R^{\mathrm{HL}}(2n; L)$ is defined in Definition 14.

4 Aggregated Pair Count Extrema Analysis

The analysis sections that follow describe empirical structure observed in the data, including higher-order regularities and qualitative trends. These observations are intended to be heuristic and descriptive, and are not required for the certification results presented later, but are inherently easier to independently verify. Only the bounds and non-crossing conditions established in the Certification section are used to support formal claims.

Global extrema of Goldbach pair counts aggregated over each primorial window are analysed. For each bin, we compare measured maxima and minima are compared against the corresponding PCGC–Goldbach bounds.

Across the full tested range $2n < 23\# \approx 2.5852 \times 10^8$, no violations occur. Moreover, the extrema trace smooth curvature envelopes consistent with the theoretical predictions, providing strong evidence that the geometric model accurately captures aggregate behaviour.

Figures 1, 2, and 3 are plots of the measured values compared to the HL–Windowed prediction lines and PCGC–Goldbach bounds for $\alpha = 1, 0.5$, and 0.015625, respectively.

Readers who find these plots visually underwhelming have not missed the point. The absence of dramatic features is itself informative.

A sharp change in curvature is clearly visible in the theoretical lower bounding curve whenever a new small prime enters the head term. This transition reflects a discrete structural update in the bound construction. Notably, no corresponding feature appears in the measured data, which remain smooth across the same transition.

Heuristic or near-fitting bounds are easy to construct, particularly when parameters are

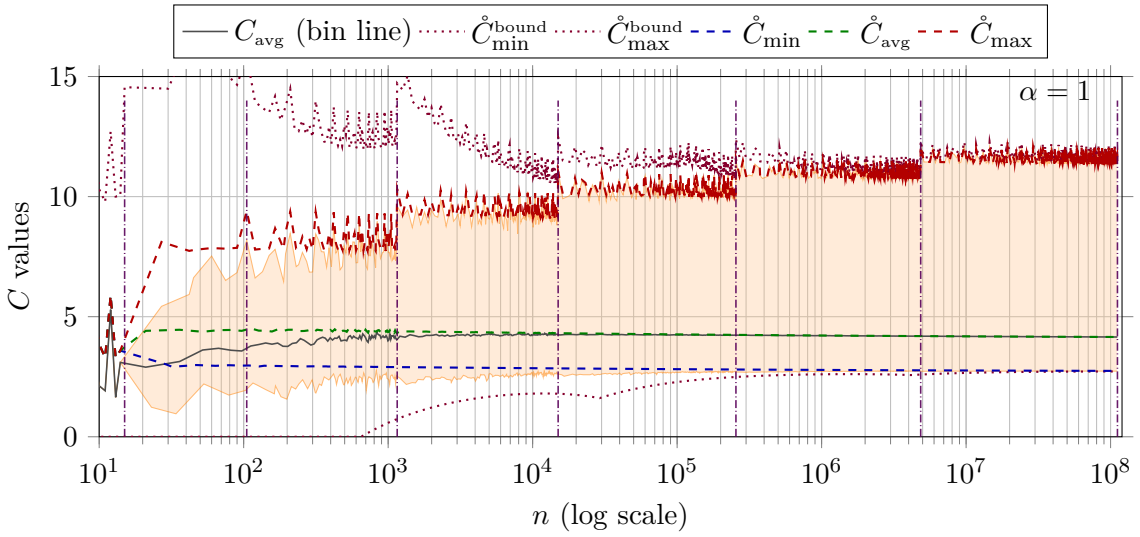

Figure 1: Scatter plots of C_{min}, C_{max}, and C_{avg} versus n with HL-A prediction lines for $\alpha = 1$. The $\mathring{C}_{\text{min}}^{\text{bound}}$ and $\mathring{C}_{\text{max}}^{\text{bound}}$ curve represents the maximum amount of cancellation that can result from small primes from PCGC–Goldbach.

freely adjusted. By contrast, parameter-free bounds that are intentionally extremely loose at small and moderate values of n, yet still tighten and converge asymptotically, are substantially more difficult to obtain.

This behaviour is essential to their validity. When Goldbach pair counts exhibit their largest relative variability, the bounds impose the weakest constraints. Conversely, as n increases and the intrinsic variability decreases, the bounds tighten asymptotically.

For example, with $\alpha = 0.5$, the theoretical onset scale n_0 for the bound is approximately 2100, whereas the measured data exhibit stable behaviour more than two orders of magnitude earlier. This substantial buffer renders the lower bound effectively trivial over most of the plotted range and ensures that early irregularities cannot threaten certification.

As a consequence, the asymptotic regime in which the geometric behaviour becomes apparent occupies only the final decades of the plots. Earlier regions are dominated by deliberate slack in the bounds rather than by meaningful geometric constraint.

The Λ-analysis of the following sections reveals the strength of the geometric model in a way that extrema plots alone cannot.

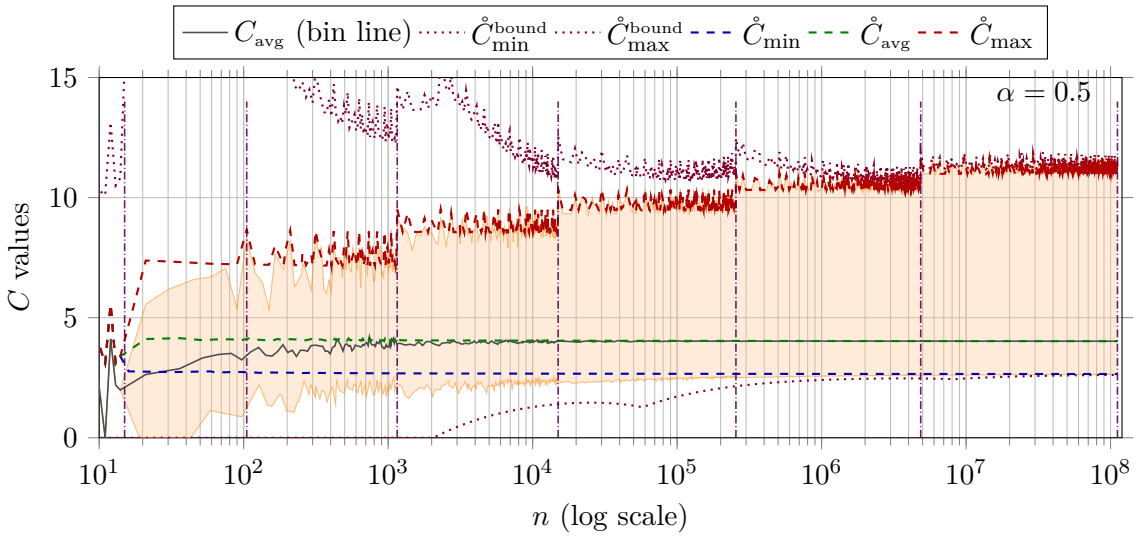

Figure 2: Scatter plots of C_{min}, C_{max}, and C_{avg} versus n with HL-A prediction lines for $\alpha = 0.5$. The $\mathring{C}_{\text{min}}^{\text{bound}}$ and $\mathring{C}_{\text{max}}^{\text{bound}}$ curve represents the maximum amount of cancellation that can result from small primes from PCGC–Goldbach.

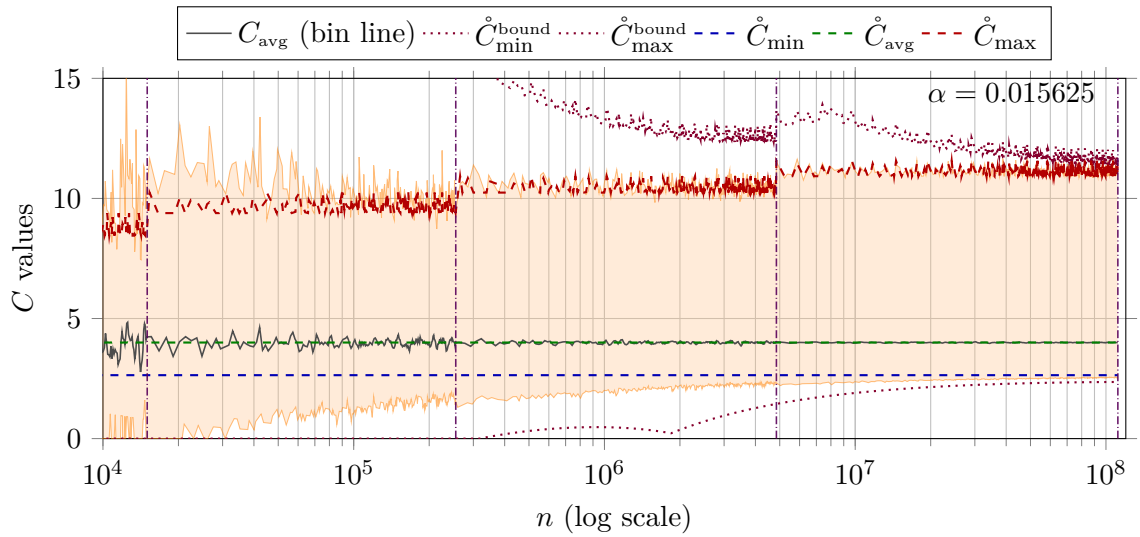

Figure 3: Scatter plots of C_{min}, C_{max}, and C_{avg} versus n with HL-A prediction lines for $\alpha = 0.015625$. The $\mathring{C}_{\text{min}}^{\text{bound}}$ and $\mathring{C}_{\text{max}}^{\text{bound}}$ curve represents the maximum amount of cancellation that can result from small primes from PCGC–Goldbach.

4.1 Definition of the Empirical Range Statistic

For each primorial bin $B_{j,p\#}$, the Hardy–Littlewood–normalized Goldbach counts are considered. Within each bin $B_{j,p\#}$, let

$$n_{\min}^{j,p\#,\alpha} \in \arg\min_{n\in B_{j,p\#}} C(2n;n\alpha), \qquad n_{\max}^{j,p\#,\alpha} \in \arg\max_{n\in B_{j,p\#}} C(2n;n\alpha), \tag{40}$$

denote values of n at which the normalized count attains its minimum and maximum, respectively. The corresponding measured extrema measurements are defined as

$$C_{\min}^{j,p\#}(\alpha) := \frac{G(2n_{\min}^{j,p\#,\alpha};n\alpha)\log^2 n_{\min}^{j,p\#,\alpha}}{n\alpha}, \tag{41}$$

$$C_{\max}^{j,p\#}(\alpha) := \frac{G(2n_{\max}^{j,p\#,\alpha};n\alpha)\log^2 n_{\max}^{j,p\#,\alpha}}{n\alpha}. \tag{42}$$

The associated bound predictions, evaluated over the same bin, are defined by

$$\mathring{C}_{\min}^{\mathrm{bound},j,p\#}(\alpha) := \min_{n\in B_{j,p\#}} \left(\mathring{G}^{\mathrm{HL}}(2n;n\alpha) - R^{\mathrm{HL}}(2n;\sqrt{2n\alpha})\right)\frac{\log^2 n}{n\alpha}, \tag{43}$$

$$\mathring{C}_{\max}^{\mathrm{bound},j,p\#}(\alpha) := \max_{n\in B_{j,p\#}} \left(\mathring{G}^{\mathrm{HL}}(2n;n\alpha) + R^{\mathrm{HL}}(2n;\sqrt{2n\alpha})\right)\frac{\log^2 n}{n\alpha}. \tag{44}$$

then the logarithmic deviations are defined as

$$\Lambda_{\min}^{\mathrm{bound},j,p\#}(\alpha) := \log\left(\frac{C_{\min}^{j,p\#}(\alpha)}{\mathring{C}_{\min}^{\mathrm{bound},j,p\#}(\alpha)}\right), \qquad \Lambda_{\max}^{\mathrm{bound},j,p\#}(\alpha) := \log\left(\frac{C_{\max}^{j,p\#}(\alpha)}{\mathring{C}_{\max}^{\mathrm{bound},j,p\#}(\alpha)}\right). \tag{45}$$

To visualize finite-scale variability while suppressing bin-to-bin noise, we enumerate all primorial bins $B_{j,p\#}$ in increasing order of their left endpoints and denote the resulting ordered sequence by $\{B_k\}_{k\geq 0}$. This ordering may cross primorial boundaries. For each k, the quantities $\Lambda_{\min}^{\mathrm{bound},k}(\alpha)$ and $\Lambda_{\max}^{\mathrm{bound},k}(\alpha)$ are defined to be the corresponding values associated with the bin B_k.

Then group consecutive bins into blocks of fixed size. For each block index $\ell \geq 0$, the interval is defined as

$$\mathcal{K}_\ell := \{\, k : 12\ell \leq k < 12(\ell+1) \,\}. \tag{46}$$

The range extrema over each block are defined as

$$\Lambda_{\min}^{\mathrm{low},\ell}(\alpha) := \min_{k\in\mathcal{K}_\ell} \Lambda_{\min}^{\mathrm{bound},k}(\alpha), \qquad \Lambda_{\min}^{\mathrm{high},\ell}(\alpha) := \max_{k\in\mathcal{K}_\ell} \Lambda_{\min}^{\mathrm{bound},k}(\alpha), \tag{47}$$

$$\Lambda_{\max}^{\mathrm{low},\ell}(\alpha) := \min_{k\in\mathcal{K}_\ell} \Lambda_{\max}^{\mathrm{bound},k}(\alpha), \qquad \Lambda_{\max}^{\mathrm{high},\ell}(\alpha) := \max_{k\in\mathcal{K}_\ell} \Lambda_{\max}^{\mathrm{bound},k}(\alpha). \tag{48}$$

The corresponding n-values plotted on the horizontal axis are taken to be the values $n^k_{\min}$ and $n^k_{\max}$ at which these extremal deviations occur within each block. Thus, each range block summarizes the spread of the deviations $\Lambda^{\text{bound},k}_{\min}$ and $\Lambda^{\text{bound},k}_{\max}$ over a fixed collection of consecutive primorial bins, rather than representing a pointwise interval at a single value of n.

Remark (Choice of Block Size). The block size of 12 consecutive primorial bins was chosen for pragmatic and statistical reasons. First, sample sizes on the order of ten are commonly regarded as a minimal scale at which dispersion statistics become stable, even in non-Gaussian settings. Second, grouping bins at this scale provides sufficient data reduction to allow multiple range bands to be displayed simultaneously without obscuring large-scale structure. Empirically, smaller block sizes lead to visually noisy envelopes, while larger block sizes suppress finite-scale features that remain relevant to the interpretation of the data.

4.2 Minimum Geometric Bounds

Figure 4 plots eleven representative summary ranges for $\Lambda^{\text{bound},k}_{\min}$. PCGC–Goldbach predicts that these curves approach zero asymptotically, but it does not impose strong restrictions on their detailed shape beyond the requirement that the corresponding ratios remain strictly non-negative. The observed overall decreasing trend is consistent with the predictions of PCGC–Goldbach.

The constants defining $\widehat{R}^{\text{HL}}$ are chosen so that

$$\widehat{R}^{\text{HL}}(2n; \mathcal{Q}_p(n)) = R^{\text{HL}}(2n; \mathcal{Q}_p(n)) \qquad \forall\, n \in \mathbb{N}, \quad \forall\, p \in \mathbb{P}_{\text{eff}}(n). \tag{49}$$

Since $\widehat{R}^{\text{HL}}(2n; L)$ decreases monotonically with n, for all 81 values of α we plot $\Lambda^{\text{bound}}_{\min}$ using

$$L \approx \mathcal{Q}_p(n), \qquad 3 \mid n, \qquad p \in \{11, 13\}. \tag{50}$$

To avoid division by zero and undefined values of $\log(0)$, such cases are treated as unplottable. The approximation is taken to be the closest available value to equality. If no plottable value exists on both sides of the target $\mathcal{Q}_p(n)$, the corresponding point is also considered unplottable.

Figure 5 plots all 81 values of α. The smallest α-values due to low statistics exhibit excessive finite-scale variability (jitter), making it difficult to confirm a monotonic trend. For the remaining values of α, the curves are clearly decreasing. Table 1 lists representative values for twelve selected α-levels. The table includes all α values that are powers of 2 (i.e., 2^{-n} for integer n), together with the second lowest α value to illustrate the change in standard deviation.

Since $R^{\mathrm{HL}} \geq |\varepsilon|$, and the plotted quantities are only loosely tied to the scale $|\varepsilon|$, strict inequalities and asymptotic convergence are required only once squeezed sufficiently by the upper and lower bounds. Nevertheless, the observed decreasing trend provides additional empirical support for the conjecture.

Including unplottable data, the inequality $R^{\mathrm{HL}} \geq |\varepsilon|$ holds without exception across the entire computed range.

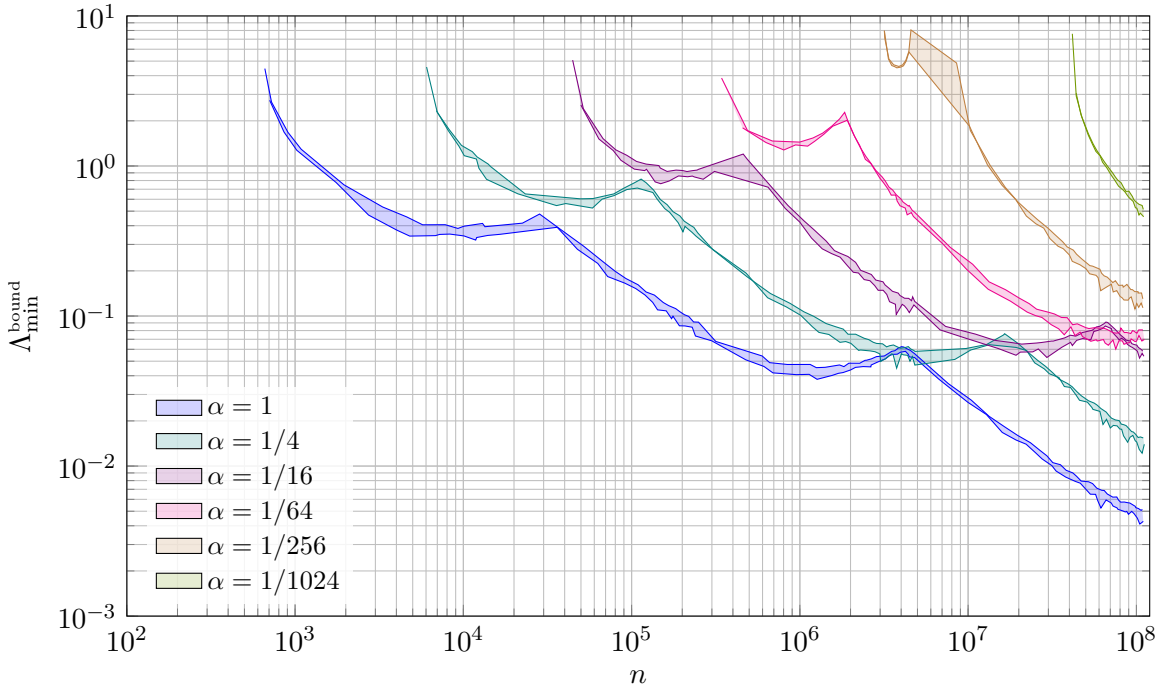

Figure 4: Smooth envelope bands for $\Lambda_{\min}^{\mathrm{bound}}$ by α.

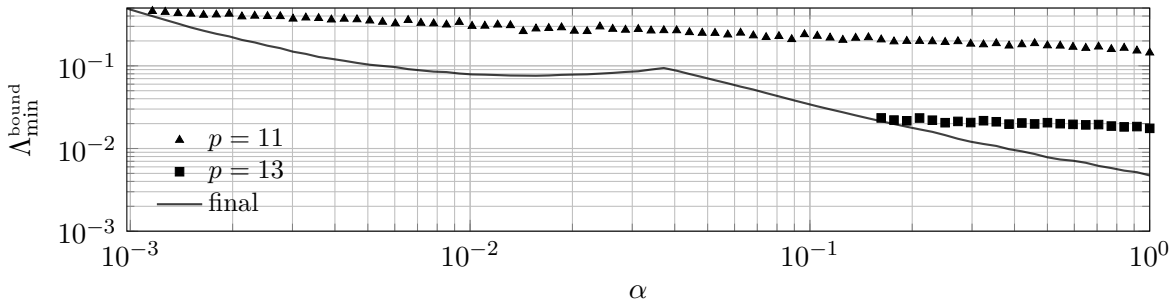

Figure 5: All α values showing event and final envelope $\Lambda_{\min}^{\mathrm{bound}}$ statistics.

Table 1: Selected α values showing event and final envelope $\Lambda_{\min}^{\text{bound}}$ statistics.

α	p=11	p=13	final $\pm$ std.dev.
0.0009765625	nan	nan	$4.94 \cdot 10^{-1} \pm 1.48 \cdot 10^{-2}$
0.001064948958	$5.05 \cdot 10^{-1}$	nan	$4.43 \cdot 10^{-1} \pm 1.36 \cdot 10^{-2}$
0.001953125	$4.25 \cdot 10^{-1}$	nan	$2.27 \cdot 10^{-1} \pm 7.42 \cdot 10^{-3}$
0.00390625	$3.61 \cdot 10^{-1}$	nan	$1.22 \cdot 10^{-1} \pm 5.21 \cdot 10^{-3}$
0.0078125	$3.25 \cdot 10^{-1}$	nan	$8.51 \cdot 10^{-2} \pm 5.63 \cdot 10^{-3}$
0.015625	$2.82 \cdot 10^{-1}$	nan	$7.58 \cdot 10^{-2} \pm 3.40 \cdot 10^{-3}$
0.03125	$2.78 \cdot 10^{-1}$	nan	$8.59 \cdot 10^{-2} \pm 1.96 \cdot 10^{-3}$
0.0625	$2.51 \cdot 10^{-1}$	nan	$5.60 \cdot 10^{-2} \pm 1.29 \cdot 10^{-3}$
0.125	$2.05 \cdot 10^{-1}$	nan	$2.74 \cdot 10^{-2} \pm 8.30 \cdot 10^{-4}$
0.25	$1.93 \cdot 10^{-1}$	$2.05 \cdot 10^{-2}$	$1.45 \cdot 10^{-2} \pm 3.70 \cdot 10^{-4}$
0.5	$1.76 \cdot 10^{-1}$	$2.05 \cdot 10^{-2}$	$7.83 \cdot 10^{-3} \pm 4.20 \cdot 10^{-4}$
1	$1.44 \cdot 10^{-1}$	$1.75 \cdot 10^{-2}$	$4.72 \cdot 10^{-3} \pm 2.50 \cdot 10^{-4}$

4.3 Maximum Geometric Bounds

The complementary analysis for the upper geometric bounds is done next. All definitions, binning conventions, and range constructions are exactly as in the preceding subsection, with $\Lambda_{\max}^{\text{bound},k}$ replacing $\Lambda_{\min}^{\text{bound},k}$. Accordingly, only the behaviour of the resulting range summaries and their consistency with the predictions of PCGC–Goldbach are considered.

Figure 6 plots eleven representative summary ranges for $\Lambda_{\max}^{\text{bound},k}$. As in the lower-bound case, PCGC–Goldbach predicts eventual convergence toward zero, while imposing no detailed constraints on the intermediate shape of the curves beyond positivity of the underlying ratios. The observed envelopes exhibit the same overall decreasing trend, consistent with this prediction.

The plotting procedure mirrors that used for the minimum bounds. Since $\widehat{R}^{\text{HL}}(2n; L)$ is monotone in n, the approximation $L \approx \mathcal{Q}_p(n)$ is again employed, with the same restrictions on admissible values of n and the same criteria for excluding unplottable points. Figure 7 displays the full set of 81 α-values. As before, the smallest values of α are dominated by finite-scale variability, while the remaining curves show a clear decreasing trend. Table 2 lists representative values for twelve selected α-levels.

Including unplottable data, no violations of the inequality $R^{\text{HL}} \geq |\varepsilon|$ are observed across the entire computed range.

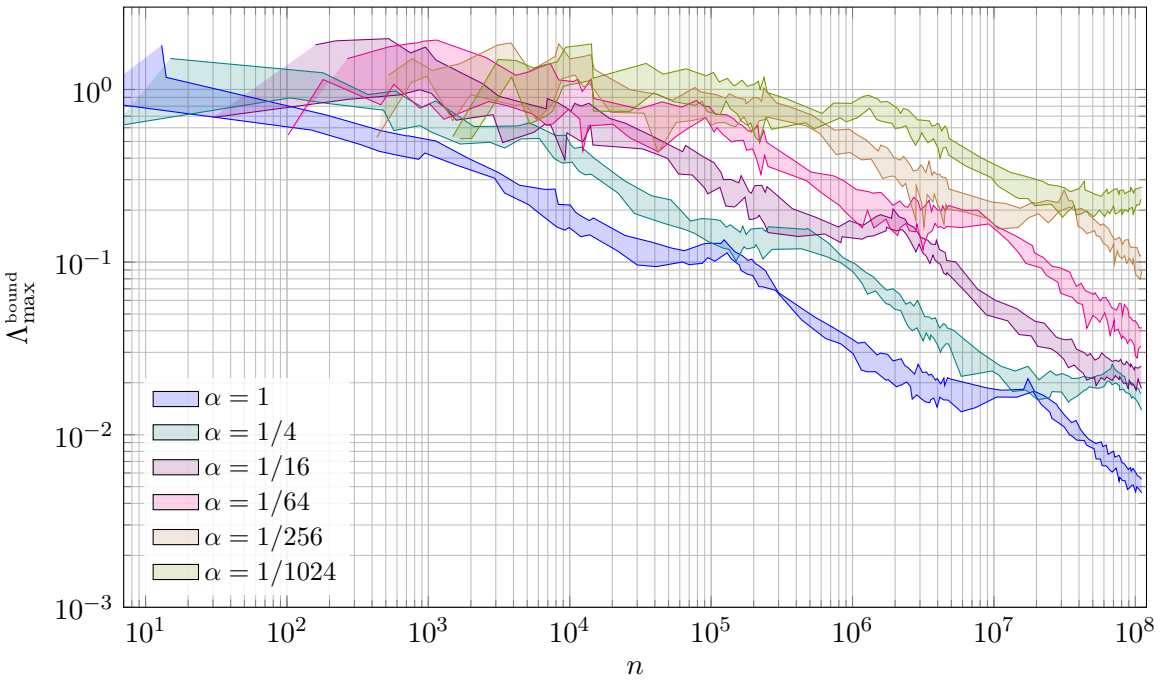

Figure 6: Smooth envelope bands for $\Lambda_{\max}^{\text{bound}}$ by α.

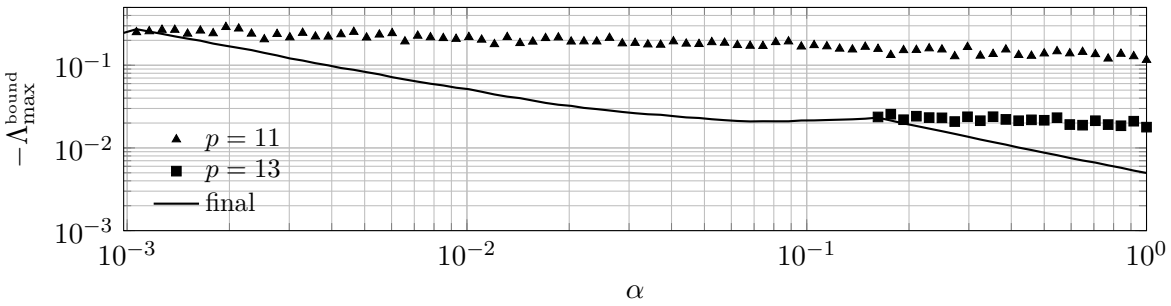

Figure 7: All α values showing event and final envelope $\Lambda_{\max}^{\text{bound}}$ statistics.

Table 2: Selected α values showing event and final envelope $\Lambda_{\max}^{\text{bound}}$ statistics.

α	p=11	p=13	final $\pm$ std.dev.
0.0009765625	nan	nan	$-2.46 \cdot 10^{-1} \pm 1.24 \cdot 10^{-2}$
0.001064948958	$-2.51 \cdot 10^{-1}$	nan	$-2.73 \cdot 10^{-1} \pm 1.15 \cdot 10^{-2}$
0.001953125	$-2.89 \cdot 10^{-1}$	nan	$-1.72 \cdot 10^{-1} \pm 1.04 \cdot 10^{-2}$
0.00390625	$-2.22 \cdot 10^{-1}$	nan	$-9.97 \cdot 10^{-2} \pm 7.14 \cdot 10^{-3}$
0.0078125	$-2.17 \cdot 10^{-1}$	nan	$-5.98 \cdot 10^{-2} \pm 4.36 \cdot 10^{-3}$
0.015625	$-1.93 \cdot 10^{-1}$	nan	$-3.74 \cdot 10^{-2} \pm 2.45 \cdot 10^{-3}$
0.03125	$-1.86 \cdot 10^{-1}$	nan	$-2.63 \cdot 10^{-2} \pm 2.37 \cdot 10^{-3}$
0.0625	$-1.75 \cdot 10^{-1}$	nan	$-2.12 \cdot 10^{-2} \pm 1.74 \cdot 10^{-3}$
0.125	$-1.58 \cdot 10^{-1}$	nan	$-2.20 \cdot 10^{-2} \pm 1.07 \cdot 10^{-3}$
0.25	$-1.55 \cdot 10^{-1}$	$-2.31 \cdot 10^{-2}$	$-1.59 \cdot 10^{-2} \pm 9.60 \cdot 10^{-4}$
0.5	$-1.39 \cdot 10^{-1}$	$-2.16 \cdot 10^{-2}$	$-8.76 \cdot 10^{-3} \pm 4.50 \cdot 10^{-4}$
1	$-1.16 \cdot 10^{-1}$	$-1.78 \cdot 10^{-2}$	$-4.98 \cdot 10^{-3} \pm 2.60 \cdot 10^{-4}$

4.4 Origin of the Structured Envelope Curves

The non-monotone structure visible in the range envelopes is not an artifact of the aggregation procedure, but a genuine feature of the prediction geometry. Its origin may be understood heuristically from the residue-based formulation introduced in [6].

The prediction function is ultimately governed by residue classes modulo small primes, with the underlying density model justified by Dirichlet's Theorem on arithmetic progressions [1]. In the asymptotic limit, all admissible residue classes are expected to occur with equal frequency, yielding a smooth limiting contribution to the Hardy–Littlewood correction factors.

To model finite-scale behaviour, a Chinese Remainder Theorem-like threshold is introduced [3] to separate primes whose residue distributions may be regarded as effectively uniform from those whose contributions have not yet stabilized. Primes below this threshold are treated as fully equidistributed and contribute to a smooth base term. Primes above the threshold are grouped into an exponential tail, whose net effect decays rapidly as the scale increases.

As the scale parameter grows, this exponential tail contracts, causing the predicted bounds to tighten exponentially. However, whenever a new prime crosses below the CRT-like threshold, the structure of the residue product changes discretely. This transition resets the tail decomposition and produces a localized relaxation in the prediction envelope. The resulting alternation between exponential tightening and discrete re-normalization gives rise to the observed periodic modulation in the prediction curves.

The measured values do not exhibit the same sharp periodic structure. This is expected: higher-order correlations beyond the leading residue model, together with the blockwise aggregation used to construct the range envelopes, act to smooth the empirical curves. Consequently, the prediction envelopes display clear modular interference patterns, while the measured ranges converge more uniformly toward the asymptotic limit.

5 Pointwise Pair Count Analysis

Pointwise analysis for the purpose of certifying the conjecture across all validation checks follows.

For each admissible n, we evaluate 81 distinct windowed pair counts, corresponding to the discrete scale parameters

$$\alpha_i := 2^{-i/8}, \qquad i = 0, 1, \ldots, 80. \tag{51}$$

this set of scale parameters is set as

$$\mathcal{A} := \{\, \alpha_i : i = 0, 1, \ldots, 80 \,\}. \tag{52}$$

For each $\alpha \in \mathcal{A}$, both the upper and lower bounds are tested independently.

Within each primorial bin, the measured value that approaches its bound most closely is identified. In all cases, no crossings are observed. Rather than exhibiting monotonic convergence, the extremal deviations display bounded local fluctuations while remaining confined within the predicted envelope and trending toward the asymptotic λ values. This behaviour supports the interpretation of the bounds as genuine geometric constraints rather than statistical envelopes.

Due to storage limitations, predicted bounds and measured counts must be generated jointly in this mode. The combined computation requires approximately 60 days on an Apple M2 processor, with up to 12 concurrent processes running continuously.

5.1 Definition of the Empirical Range Statistic

Define the logarithmic deviations

$$\lambda_{\min}^{j,p\#}(\alpha) := \min_{n \in B_{j,p\#}} \log\left(\frac{G(2n; n\alpha)}{\mathring{G}^{\mathrm{HL}}(2n; \sqrt{2n\alpha}) - R^{\mathrm{HL}}(2n; \sqrt{2n\alpha})} \right), \tag{53}$$

$$\lambda_{\max}^{j,p\#}(\alpha) := \max_{n \in B_{j,p\#}} \log\left(\frac{G(2n; n\alpha)}{\mathring{G}^{\mathrm{HL}}(2n; \sqrt{2n\alpha}) + R^{\mathrm{HL}}(2n; \sqrt{2n\alpha})} \right). \tag{54}$$

To visualize finite-scale variability while suppressing bin-to-bin noise, all primorial bins $B_{j,p\#}$ in increasing order of their left endpoints and denote the resulting ordered sequence by $\{B_k\}_{k\geq 0}$ are enumerated. This ordering may cross primorial boundaries. For each k, the quantities $\lambda_{\min}^{k}(\alpha)$ and $\lambda_{\max}^{k}(\alpha)$ are defined to be the corresponding values associated with the bin B_k.

Then consecutive bins into blocks are aggregated in fixed sized groups. For each block index $\ell \geq 0$, intervals are defined as

$$\mathcal{K}_\ell := \{\, k : 12\ell \leq k < 12(\ell + 1) \,\}. \tag{55}$$

Then, the range extrema over each block are defined as

$$\lambda_{\min}^{\mathrm{low},\ell}(\alpha) := \min_{k \in \mathcal{K}_\ell} \lambda_{\min}^{k}(\alpha), \qquad \lambda_{\min}^{\mathrm{high},\ell}(\alpha) := \max_{k \in \mathcal{K}_\ell} \lambda_{\min}^{k}(\alpha), \tag{56}$$

$$\lambda_{\max}^{\mathrm{low},\ell}(\alpha) := \min_{k \in \mathcal{K}_\ell} \lambda_{\max}^{k}(\alpha), \qquad \lambda_{\max}^{\mathrm{high},\ell}(\alpha) := \max_{k \in \mathcal{K}_\ell} \lambda_{\max}^{k}(\alpha). \tag{57}$$

The corresponding n-values plotted on the horizontal axis are taken to be the values $n^k_{\min}$ and $n^k_{\max}$ at which these extremal deviations occur within each block. Thus, each range block summarizes the spread of the pointwise deviations $\lambda^k_{\min}$ and $\lambda^k_{\max}$ over a fixed collection of consecutive primorial bins, rather than representing an interval at a single value of n.

5.2 Pointwise Minimum Bounds

The pointwise minimum deviations $\lambda^k_{\min}(\alpha)$, aggregated into range summaries as defined in the previous subsection are examined. In contrast to the geometric bounds, these quantities reflect local (pointwise) behaviour prior to any block-level aggregation.

Figure 8 plots representative range envelopes for $\lambda^k_{\min}(\alpha)$. As predicted by PCGC–Goldbach, these values remain non-negative and exhibit an overall downward trend. Notably, the fluctuations are less pronounced than in the geometric case. This reflects the fact that the geometric aggregation procedure inflates the effective bounds and, with them, the apparent variability.

The plotting conventions, admissibility criteria, and handling of unplottable points are identical to those used previously. Figure 9 displays all 81 α-values. As before, the smallest values of α are dominated by finite-scale effects, while the remaining curves show clear decay. Table 3 lists representative values for twelve selected α-levels.

Including unplottable data, no violations of the inequality $R^{\mathrm{HL}} \geq |\varepsilon|$ are observed across the entire computed range.

Table 3: Selected α values showing event and final envelope $\lambda_{\min}$ statistics.

α	p=11	p=13	final $\pm$ std.dev.
0.0009765625	nan	nan	$2.73 \cdot 10^{-1} \pm 1.18 \cdot 10^{-2}$
0.001064948958	$2.63 \cdot 10^{-1}$	nan	$3.00 \cdot 10^{-1} \pm 1.25 \cdot 10^{-2}$
0.001953125	$2.63 \cdot 10^{-1}$	nan	$1.46 \cdot 10^{-1} \pm 8.42 \cdot 10^{-3}$
0.00390625	$2.31 \cdot 10^{-1}$	nan	$6.80 \cdot 10^{-2} \pm 6.61 \cdot 10^{-3}$
0.0078125	$2.10 \cdot 10^{-1}$	nan	$3.58 \cdot 10^{-2} \pm 3.33 \cdot 10^{-3}$
0.015625	$1.92 \cdot 10^{-1}$	nan	$2.12 \cdot 10^{-2} \pm 1.80 \cdot 10^{-3}$
0.03125	$1.93 \cdot 10^{-1}$	nan	$1.51 \cdot 10^{-2} \pm 1.20 \cdot 10^{-3}$
0.0625	$1.77 \cdot 10^{-1}$	nan	$1.40 \cdot 10^{-2} \pm 9.60 \cdot 10^{-4}$
0.125	$1.54 \cdot 10^{-1}$	nan	$1.69 \cdot 10^{-2} \pm 5.00 \cdot 10^{-4}$
0.25	$1.36 \cdot 10^{-1}$	$1.78 \cdot 10^{-2}$	$1.15 \cdot 10^{-2} \pm 2.70 \cdot 10^{-4}$
0.5	$1.36 \cdot 10^{-1}$	$1.56 \cdot 10^{-2}$	$5.62 \cdot 10^{-3} \pm 1.40 \cdot 10^{-4}$
1	$1.01 \cdot 10^{-1}$	$1.44 \cdot 10^{-2}$	$2.68 \cdot 10^{-3} \pm 1.20 \cdot 10^{-4}$

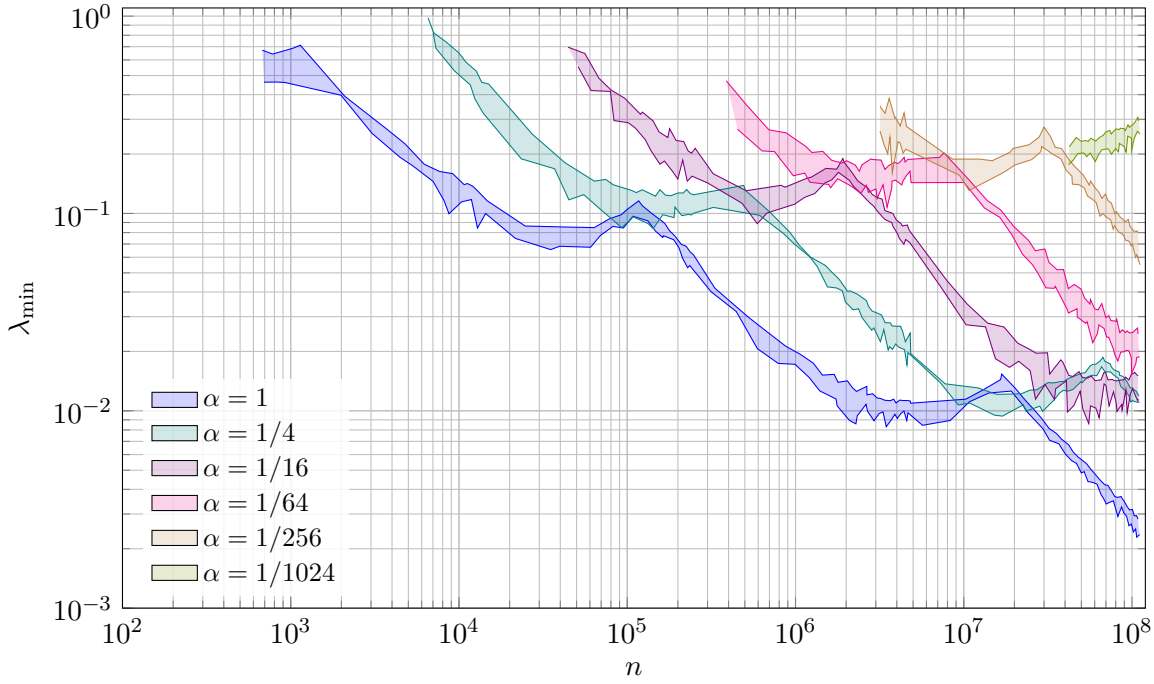

Figure 8: Smooth envelope bands for $\lambda_{\min}$ by α.

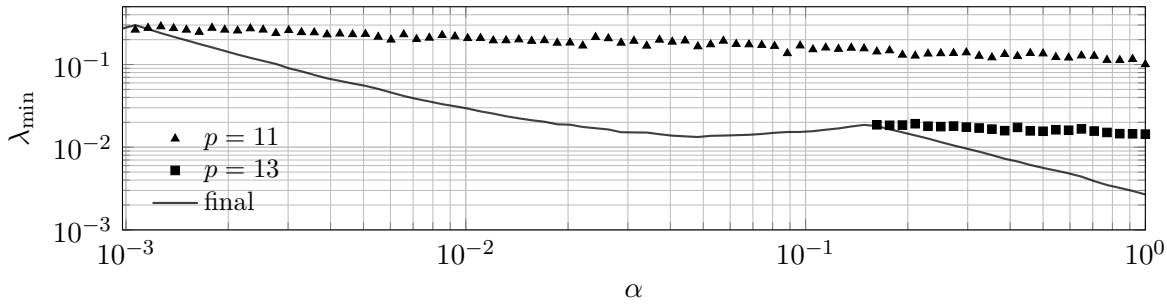

Figure 9: All α values showing event and final envelope $\lambda_{\min}$ lower statistics.

5.3 Pointwise Maximum Bounds

Consider the complementary pointwise maximum deviations $\lambda^k_{\max}(\alpha)$. These quantify local excursions above the Hardy–Littlewood prediction and provide a direct pointwise analogue of the maximum geometric bounds.

Figure 10 shows representative range envelopes for $\lambda^k_{\max}(\alpha)$. As in the minimum case, PCGC–Goldbach predicts asymptotic convergence toward zero without imposing detailed constraints on the intermediate shape. Here again, the observed fluctuations are smaller than those seen in the geometric bounds, consistent with the absence of aggregation-induced inflation.

The full collection of pointwise maximum bounds for all 81 values of α are shown in Figure 11. Finite-scale effects dominate only at the smallest values of α; for the remaining curves a clear decreasing trend is visible. Representative values are summarized in Table 4.

Including unplottable data, no violations of the inequality $R^{\mathrm{HL}} \geq |\varepsilon|$ are observed across the entire computed range.

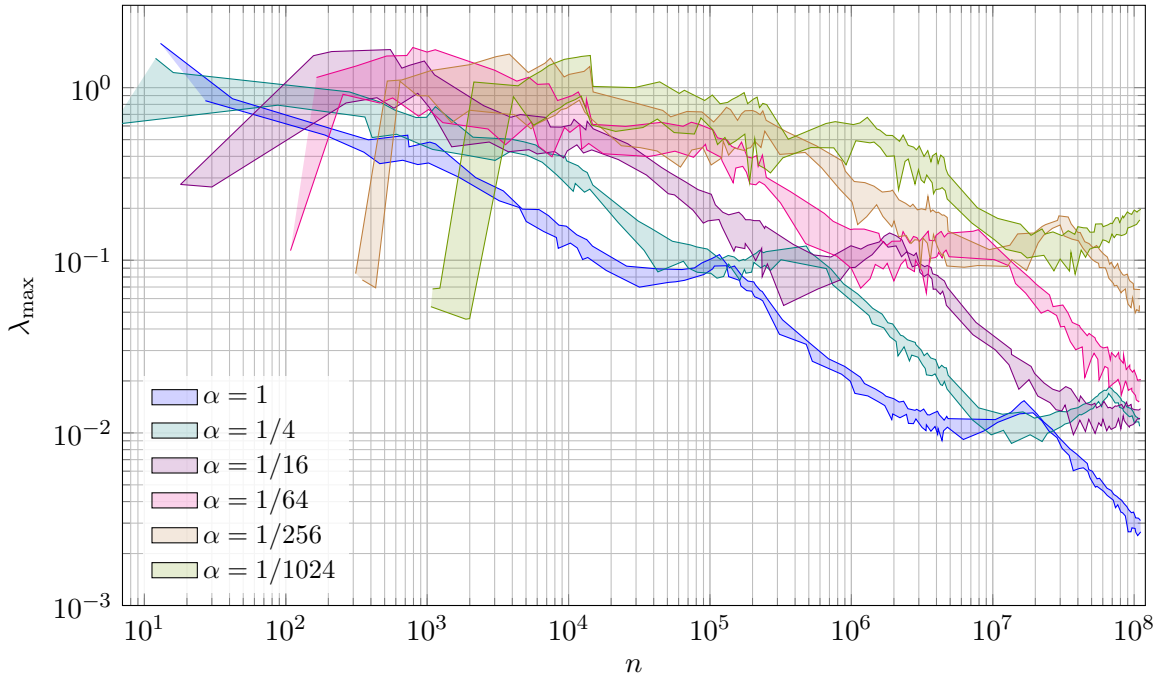

Figure 10: Smooth envelope bands for $\lambda_{\max}$ by α.

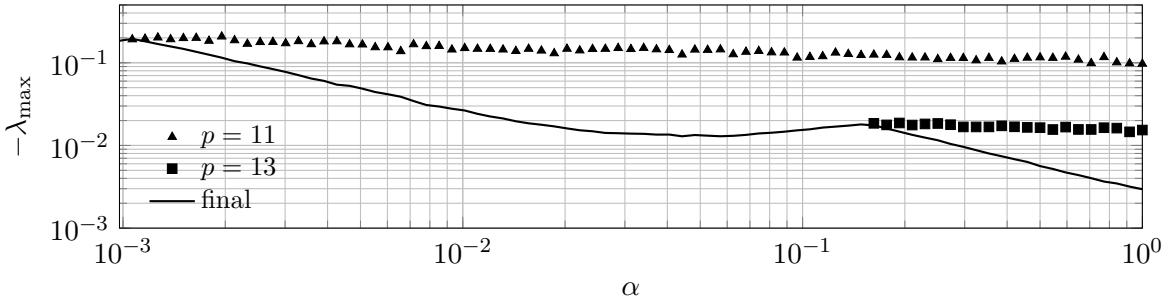

Figure 11: All α values showing event and final envelope $\lambda_{\max}$ statistics.

Table 4: Selected α values showing event and final envelope $\lambda_{\max}$ upper statistics.

α	p=11	p=13	final $\pm$ std.dev.
0.0009765625	nan	nan	$-1.85 \cdot 10^{-1} \pm 9.15 \cdot 10^{-3}$
0.001064948958	$-1.92 \cdot 10^{-1}$	nan	$-1.94 \cdot 10^{-1} \pm 8.90 \cdot 10^{-3}$
0.001953125	$-2.07 \cdot 10^{-1}$	nan	$-1.15 \cdot 10^{-1} \pm 7.12 \cdot 10^{-3}$
0.00390625	$-1.81 \cdot 10^{-1}$	nan	$-6.04 \cdot 10^{-2} \pm 4.31 \cdot 10^{-3}$
0.0078125	$-1.59 \cdot 10^{-1}$	nan	$-3.08 \cdot 10^{-2} \pm 3.39 \cdot 10^{-3}$
0.015625	$-1.47 \cdot 10^{-1}$	nan	$-1.85 \cdot 10^{-2} \pm 1.36 \cdot 10^{-3}$
0.03125	$-1.46 \cdot 10^{-1}$	nan	$-1.39 \cdot 10^{-2} \pm 1.26 \cdot 10^{-3}$
0.0625	$-1.26 \cdot 10^{-1}$	nan	$-1.31 \cdot 10^{-2} \pm 5.20 \cdot 10^{-4}$
0.125	$-1.32 \cdot 10^{-1}$	nan	$-1.69 \cdot 10^{-2} \pm 4.30 \cdot 10^{-4}$
0.25	$-1.11 \cdot 10^{-1}$	$-1.84 \cdot 10^{-2}$	$-1.16 \cdot 10^{-2} \pm 2.50 \cdot 10^{-4}$
0.5	$-1.16 \cdot 10^{-1}$	$-1.64 \cdot 10^{-2}$	$-5.63 \cdot 10^{-3} \pm 1.70 \cdot 10^{-4}$
1	$-9.72 \cdot 10^{-2}$	$-1.54 \cdot 10^{-2}$	$-2.96 \cdot 10^{-3} \pm 1.30 \cdot 10^{-4}$

6 Certification

Theorem 1 (Empirical Certification of PCGC–Goldbach Bounds Up To 23#/2)**.**
Let $\mathcal{A}$ denote the discrete set of window parameters used in the certification, as defined in equation (52). For each $\alpha \in \mathcal{A}$ and each integer $2n \geq 4$, let $G(2n; n\alpha)$ denote the measured Goldbach pair count in the window of half-width $n\alpha$, and let $\mathring{G}^{\mathrm{HL}}(2n; n\alpha)$ be the corresponding Hardy–Littlewood geometric main term. As in [6], write

$$G(2n; n\alpha) = \mathring{G}^{\mathrm{HL}}(2n; n\alpha) + \varepsilon(2n; L), \tag{58}$$

where $\varepsilon(2n; L)$ is the exact remainder term and L denotes the associated effective modulus cutoff.

Fix an admissible effective modulus cutoff $L = \mathcal{Q}(2n; \alpha)$. Let $R^{\mathrm{HL}}(2n; L)$ denote the exact geometric remainder envelope, and let $\widehat{R}^{\mathrm{HL}}(2n; L)$ denote the associated explicit bounding

envelope, as in Definitions 14 and 15, respectively.

(A) Certifiability of the envelope. For all admissible (n, L), the envelope $\widehat{R}^{\mathrm{HL}}(2n; L)$ is nonnegative, conservative, and asymptotically sharp in the sense that

$$|\varepsilon(2n; L)| \le R^{\mathrm{HL}}(2n; L) \le \widehat{R}^{\mathrm{HL}}(2n; L), \tag{59}$$

and moreover $\widehat{R}^{\mathrm{HL}}(2n; L) = R^{\mathrm{HL}}(2n; L)(1 + o_L(1))$ uniformly over the admissible parameter ranges.

(B) Empirical certification on the computed range. For every $\alpha \in \mathcal{A}$ and every integer n with

$$4 \le 2n \le 23\#, \tag{60}$$

the measured counts satisfy the certified two-sided geometric bounds

$$\mathring{G}^{\mathrm{HL}}(2n; n\alpha) - R^{\mathrm{HL}}(2n; \sqrt{2n\alpha}) \;\le\; G(2n; n\alpha) \;\le\; \mathring{G}^{\mathrm{HL}}(2n; n\alpha) + R^{\mathrm{HL}}(2n; \sqrt{2n\alpha}). \tag{61}$$

Since $\widehat{R}^{\mathrm{HL}}(2n; L) \ge R^{\mathrm{HL}}(2n; L)$ for all admissible L, by the *Overall Bounding Envelope Lemma* of [6], which establishes uniform dominance of $\widehat{R}^{\mathrm{HL}}$ over R^{HL}, the same certified inequalities hold *a fortiori* with $\widehat{R}^{\mathrm{HL}}$ in place of R^{HL}.

On the full computed range, certification is expressed by the two-sided inequality (61), which is checked directly for every (n, α) in the grid. For visualization, logarithmic ratio diagnostics on the *plottable domain* where the relevant denominators are positive (so that division and log are defined) are plotted as well. On this domain, the lower inequality implies

$$\lambda_{\min}(n; \alpha) := \log\left(\frac{G(2n; n\alpha)}{\mathring{G}^{\mathrm{HL}}(2n; n\alpha) - R^{\mathrm{HL}}(2n; L)}\right) \ge 0, \tag{62}$$

while the upper inequality implies, equivalently,

$$\lambda_{\max}(n; \alpha) := \log\left(\frac{G(2n; n\alpha)}{\mathring{G}^{\mathrm{HL}}(2n; n\alpha) + R^{\mathrm{HL}}(2n; L)}\right) \le 0. \tag{63}$$

Points excluded from plots only to avoid division by 0 or $\log(0)$ are treated as unplottable; these cases are still included in the direct verification of (61).

Proof.
Part (A) follows directly from the envelope framework developed in [6]. In particular, the *Overall Bounding Envelope Lemma* of [5] establishes that the exact remainder term satisfies

$$|\varepsilon(2n; L)| \le R^{\mathrm{HL}}(2n; L), \tag{64}$$

and that the explicit envelope $\widehat{R}^{\mathrm{HL}}(2n; L)$ uniformly dominates $R^{\mathrm{HL}}(2n; L)$ for all admissible L. The non-asymptotic-proxy nature of $\widehat{R}^{\mathrm{HL}}$ is likewise a consequence of this lemma.

For Part (B), we certify the inequalities (61) by direct computation over the full grid $\{(\alpha, n) : \alpha \in \mathcal{A},\ 4 \le n \le 23\#/2\}$. For each pair (α, n), the computational pipeline evaluates $G(2n; n\alpha)$, $\mathring{G}^{\mathrm{HL}}(2n; n\alpha)$, and $\widehat{R}^{\mathrm{HL}}(2n; \sqrt{2n\alpha})$, and explicitly checks the two inequalities in (61). All checks pass with no exceptions on the computed range. The stated nonnegativity of the plotted logarithmic deviations is equivalent to the same inequalities wherever the denominators are positive; points excluded from plots for numerical reasons were nevertheless checked against (61) and likewise show no violations.

The certified data products, executable pipeline, and verification logs used in this computation are archived and made available via the accompanying software package [4], enabling independent reproduction and audit of all certified claims. □

7 Conclusion

This work establishes an empirical certification of geometric confinement for Goldbach pair counts over the range $4 \le 2n \le 23\#$, evaluated across the discrete family of fixed-scale windows $\mathcal{A} = \{2^{-i/8} : i = 0, 1, \ldots, 80\}$. Within this domain, no violations of the certified two-sided inequalities occur, either in plotted data or in the full set of values checked but excluded from visualization for numerical reasons. In this sense, the tested range admits no empirical escape route: every measured value lies within the geometric envelopes predicted by the Prime Curvature Geometry Conjecture—Goldbach case.

A central distinction of this work is the separation between probabilistic heuristics and geometric confinement. While classical Hardy–Littlewood heuristics describe average behaviour, the present certification concerns pointwise and blockwise control by explicit geometric envelopes. The absence of violations is therefore not an assertion of likelihood or statistical typicality, but a falsifiable geometric statement verified over a finite, explicitly enumerated domain.

The certification framework employed here is deliberately reproducible. All claims are grounded in direct computation over a fully specified grid of parameters, with archived data products, executable pipelines, and verification logs enabling independent audit. In this respect, certification is treated not as an informal observational claim, but as a concrete experimental standard: any counterexample within the tested regime would be detectable, reproducible, and decisive.

It is important to delineate the scope of this result. The present analysis is restricted to fixed-scale Goldbach windows indexed by constant α, organized using primorial-based

binning. No claims are made regarding short-interval regimes in the offset variable m, including windows of fixed or slowly growing size. Such regimes are geometrically distinct and would require a different experimental design, coverage strategy, and certification criterion than those used here.

Although one could, in principle, project certified points from the fixed-scale α_i lines onto shorter interval regimes, such projections are inherently loose and do not constitute meaningful short interval certification. At best, they provide consistency checks rather than independent validation. A serious short-interval analysis would instead require tracing a family of scale functions $\alpha(n)$ across the full data range, with bounds evaluated pointwise along these dynamically varying trajectories. That problem lies outside the scope of the present in this paper.

Within its stated domain, however, the conclusion is unambiguous: across all tested scales and throughout the full certified range, the Goldbach pair counts exhibit no empirical deviations from the geometric constraints predicted by the Prime Curvature Geometry Conjecture.

7.1 Outlook and Open Directions

The present work establishes certified geometric bounds for primorial-based window families over a fixed-scale parameter grid. Several natural extensions suggest themselves, particularly in regimes that are not amenable to the fixed-scale framework employed here.

One such direction is the development of a dedicated certification program for short-interval behaviour in the offset variable m. While projections from the fixed-scale α_i lines are possible, such projections are inherently loose and do not support meaningful certification. A genuine short-interval analysis would instead require tracing dynamically varying scale functions $\alpha(n)$ across the full data range, with bounds certified pointwise along these trajectories.

This regime constitutes a geometrically distinct problem and would necessitate different experimental design principles and coverage strategies than those used in the present study. This is a natural and well-defined direction for future investigation.

8 Reproducibility

All empirical results and certifications reported in this paper are derived from deterministic computations over explicitly enumerated parameter grids. The full computational

pipeline—including executable code, configuration files, and verification scripts—has been archived to enable independent reproduction and audit of all certified claims.

The certification procedure does not rely on stochastic sampling, heuristic filtering, or post hoc selection. Every admissible pair (α, n) in the certified domain is evaluated explicitly, and all inequalities are checked directly. Any counterexample within the tested range would therefore be detectable and reproducible using the archived materials.

The software package associated with this work also records version information, build parameters, and platform details sufficient to reproduce the numerical results across standard computing environments.[4]

8.1 Data Availability

The certified data products generated for this study, including all evaluated Goldbach pair counts, geometric envelope values, and verification logs, are archived alongside the computational pipeline. Data are provided in machine-readable formats with documented field specifications and fixed ordering conventions.

Checksum files are included to verify data integrity, and all datasets are labelled by the corresponding parameter values (α, n) to permit independent validation of individual certified inequalities. The complete archive is available via the software repository [4] , and contains all information necessary to reproduce the figures, tables, and certification results reported in this paper.

References

[1] Tom M. Apostol. *Introduction to Analytic Number Theory*. Undergraduate Texts in Mathematics. Springer, 1976.

[2] G. H. Hardy and J. E. Littlewood. Some problems of 'Partitio Numerorum'; III: On the expression of a number as a sum of primes. *Acta Mathematica*, 44(1):1–70, 1923.

[3] Ivan Niven, Herbert S. Zuckerman, and Hugh L. Montgomery. *An Introduction to the Theory of Numbers*. Wiley, 5 edition, 1991.

[4] Bill C. Riemers. Sieve-goldbach: Source code and data for sieve-theoretic analyses of goldbach's conjecture, 2025. Version v0.2.0. Available at `https://10.5281/zenodo.18329831`.

[5] Bill C. Riemers. Sieve-theoretic reformulation of goldbach's conjecture. 2025. Available at `https://doi.org/10.5281/zenodo.18338749`.

[6] Bill C. Riemers. Prime curvature geometry and the structure of additive prime deviations. 2026. Available at `https://doi.org/10.5281/zenodo.18330293`.